Energy and Power Engineering, 2026, 18(7), 453-481
https://www.scirp.org/journal/epe
ISSN Online: 1947-3818
ISSN Print: 1949-243X

Evaluation of the Performance of Lorentz Force Based Vibrations Control of Wind Turbine Blade

Aliyu Abubakar[1]*, Mutari Hajara Ali[2]

[1]Department of Electrical and Electronics Engineering, Federal Polytechnic, Bali, Nigeria
[2]Department of Physics, Bayero University, Kano, Nigeria
Email: *babandubu@gmail.com

How to cite this paper: Abubakar, A. and Ali, M.H. (2026) Evaluation of the Performance of Lorentz Force Based Vibrations Control of Wind Turbine Blade. *Energy and Power Engineering*, **18**, 453-481.
https://doi.org/10.4236/epe.2026.187022

Received: March 13, 2026
Accepted: July 27, 2026
Published: July 30, 2026

Abstract

Wind turbine blade vibrations induced by unsteady aerodynamic loading remain a critical challenge in modern wind energy systems, affecting efficiency, structural integrity, and service life. These effects are amplified under gusty and turbulent wind conditions, leading to higher stress levels and reduced operational reliability. Although several damping strategies exist, conventional systems are often constrained by added mass, slow transient response, high energy consumption, and maintenance requirements, while inconsistent modeling approaches hinder fair comparison. In response to these challenges, this study developed a unified MATLAB/Simulink framework to evaluate a Lorentz torque damper against nine conventional damping techniques under identical conditions, with a focus on settling time as the primary performance metric. The results show that the Lorentz torque damper achieves a 22% - 67% reduction in settling time and a 62% - 72% reduction in RMS vibration compared with conventional systems. The model validation yielded a natural frequency of 2.212 Hz, closely matching the benchmark value of 2.100 Hz with a 5.32% error. Overall, the findings confirm that the Lorentz torque damper provides an efficient, lightweight, and cost-effective solution for enhancing wind turbine vibration control and long-term operational performance.

Keywords

Electromagnetic Damping, Lorentz Torque Damper, MATLAB/Simulink, RMS Vibration, Settling Time, Vibration Control, Wind Turbine Blades

1. Introduction

The increasing global demand for renewable energy has intensified the deployment of large-scale wind turbines for sustainable electricity generation [1]. However, as wind turbine dimensions continue to increase, blade vibration problems have become more significant due to fluctuating aerodynamic forces and harsh environmental operating conditions [2].

During operation, wind turbine blades are continuously subjected to aerodynamic disturbances such as turbulence, wind shear, vortex interaction, and gust-induced loading, all of which contribute to structural vibration within the blade system. Over prolonged operational periods, these vibrations contribute significantly to material fatigue, crack propagation, structural instability, and eventual mechanical failure of wind turbine components [3]. Excessive blade vibration also reduces aerodynamic efficiency and increases stress within drivetrain and generator systems, thereby increasing maintenance requirements and reducing turbine lifespan [4].

In an effort to reduce vibration-induced damage and improve structural stability, researchers have proposed several passive, semi-active, and active damping techniques for wind turbine applications [5]. Passive damping systems such as tuned mass dampers and tuned liquid dampers are widely adopted because of their simplicity and reliability [6]. However, they frequently introduce additional structural mass and are highly sensitive to tuning conditions. Active and semi-active damping systems offer improved adaptability and vibration suppression capability but typically require sophisticated control architectures, external power sources, and higher maintenance demands.

Despite the extensive development of vibration suppression techniques, direct performance comparison remains difficult because many existing studies utilize different excitation conditions, dynamic models, and evaluation metrics [7]. Moreover, conventional damping systems often involve trade-offs between vibration suppression efficiency, added structural mass, operational energy consumption, and maintenance complexity [8].

Against this background, the present study proposes a Lorentz torque-based electromagnetic damper capable of generating contactless and velocity-dependent damping torque for effective wind turbine blade vibration suppression. A unified MATLAB/Simulink framework is developed to compare the performance of the proposed damper against nine conventional damping systems under identical operating conditions. The study focuses on evaluating transient response, RMS vibration suppression, energy efficiency, added mass effects, maintenance demand, and economic feasibility.

2. System Modeling and Damping Framework

A coupled blade-generator system is modeled as a second-order rotational dynamic system within the MATLAB/Simulink environment [9]. All damping techniques are implemented using identical excitation conditions to ensure objective and consistent comparative evaluation [10].

2.1. Wind Turbine Blade Dynamics

The dynamic behavior of the wind turbine blade is governed by inertia, damping, stiffness, and externally applied torques [11]. The governing equation of motion is expressed as [12]:

$$J_b\ddot{\theta} + B_b\dot{\theta} + k_b\theta = T_{gust} \tag{1}$$

Applying the Laplace transform yields the transfer function:

$$\frac{\theta(s)}{T_{gust}} = \frac{1}{J_b s^2 + B_b s + k_b} \tag{2}$$

The transfer function represents the blade response to external excitation in the frequency domain and forms the basis for comparative vibration analysis [13].

2.2. Generator Torque Dynamics

Generator torque dynamics are incorporated to account for electromechanical interaction between the blade system and the generator shaft [14]. The governing equation is given by [15]:

$$J\ddot{\theta} = T_m - T_e - B\dot{\theta}(3) \tag{3}$$

The generator transfer function is expressed as:

$$\frac{\theta(s)}{T_m - T_e} = \frac{1}{Js^2 + Bs} \tag{4}$$

Symbol	Definition	Unit
J_b	Blade rotational inertia	kg·m^2
B_b	Blade structural damping coefficient	N·m·s/rad
K_b	Blade stiffness	N·m/rad
θ	Blade angular displacement	rad
$\dot{\theta}$	Blade angular velocity	rad/s
$\ddot{\theta}$	Blade angular acceleration	rad/s^2
T_{gust}	Gust-induced torque	N·m
s	Laplace complex variable	—
J_g	Generator rotational inertia	kg·m^2
B_g	Generator viscous friction coefficient	N·m·s/rad
(T_m)	Mechanical torque from wind	N·m
(T_e)	Electrical torque	N·m
(θ_g)	Generator shaft angular displacement	rad

2.3. Damping Systems Considered

The study evaluates nine conventional damping techniques alongside the proposed Lorentz torque damper using identical blade-generator dynamics [16].

2.3.1. Tuned Mass Damper (TMD)

The tuned mass damper utilizes an auxiliary mass connected to the primary blade structure through a spring-damper mechanism [17]. The governing equation is [18]

$$J\ddot{\theta} + B\dot{\theta} + K\theta + c_t\left(\dot{\theta} - \dot{x}_t\right) + k_t\left(\theta - x_t\right) = T_{gust} \tag{5}$$

$$\text{and} \quad m_t\ddot{x}_t + c_t\left(\dot{x}_t - \dot{\theta}\right) + k_t\left(x_t - \theta\right) = 0 \tag{6}$$

The transfer function is:

$$\frac{\theta(s)}{T_{gust}} = \frac{m_t s^2 + c_t s + k_t}{\left(s^2 + Bs + K\right)\left(m_t s^2 + c_t s + k_t\right) - \left(c_t s - k_t\right)^2} \tag{7}$$

Symbol	Definition	Unit
θ	Blade angular displacement	rad
$\dot{\theta}$	Blade angular velocity	rad/s
$\ddot{\theta}$	Blade angular acceleration	rad/s^2
x_t	Displacement of tuned mass (TMD)	m or rad
$\dot{x}_t$	Velocity of tuned mass	m/s or rad/s
$\ddot{x}_t$	Acceleration of tuned mass	m/s^2 or rad/s^2
$\theta(s)$	Laplace transform of blade angular displacement	rad

2.3.2. Active Frictional Clutch Damper

The active frictional clutch damper suppresses vibration using controllable friction torque [19]. The active frictional clutch damper mitigates vibration by engaging friction plates to generate controllable resistance against blade motion [20]. Its damping action is governed by torque-velocity relationships that regulate the frictional force applied during operation. The system is characterized by torque-velocity relationships governing the damping effect [21].

$$J\ddot{\theta} + \left(B_b + c_f\right)\dot{\theta} + K\theta = T_{gust} \tag{8}$$

The transfer function of the active frictional clutch damper is expressed as follows:

$$\frac{\theta(s)}{T_{gust}(s)} = \frac{1}{Js^2 + \left(B_b + c_f\right)s + K_b} \tag{9}$$

Symbol	Definition	Unit
J	Equivalent rotational inertia of blade system	kg·m^2
J_b	Blade rotational inertia	kg·m^2
J_f	Flywheel inertia (rotational inertia damper)	kg·m^2
m_t	Tuned auxiliary mass (TMD)	kg

Continued

B	Structural damping coefficient of blade	N·m·s/rad
B_b	Blade viscous damping coefficient	N·m·s/rad
K	Blade stiffness coefficient	N·m/rad
K_b	Blade stiffness coefficient	N·m/rad
c_t	Damping coefficient of tuned mass damper (TMD)	N·m·s/rad
k_t	Spring stiffness of tuned mass damper (TMD)	N·m/rad

2.3.3. Active Hydraulic Damper

The hydraulic damper dissipates vibrational energy through controlled hydraulic fluid flow [22].

$$J\ddot{\theta}+\left(B_b+c_{AH}\right)\dot{\theta}+\left(K_b+K_{AH}\right)\theta=T_{gust} \tag{10}$$

The corresponding transfer function is

$$\frac{\theta(s)}{T_{gust}(s)}=\frac{1}{s^2+\left(B_b+c_{AH}\right)s+\left(K_b+K_{AH}\right)} \tag{11}$$

2.3.4. Electromagnetic Damper

The electromagnetic damper operates through eddy-current-induced resistive torque [23]. The electromagnetic damper operates on the principle that motion of a conductor within a magnetic field induces eddy currents that generate a resistive torque opposing motion [24]. This mechanism provides smooth, non-contact vibration control without direct mechanical contact. This provides smooth, non-contact vibration control [25].

$$J\ddot{\theta}+\left(B+c_{ED}\right)\dot{\theta}+K\theta=T_{gust} \tag{12}$$

The transfer function of the electromagnetic damper is expressed as follows:

$$\frac{\theta(s)}{T_{gust}(s)}=\frac{1}{Js^2+\left(B+c_{ED}\right)s+K} \tag{13}$$

2.3.5. Active Piezoelectric Damper

The active piezoelectric damper converts structural strain into electrical actuation for vibration suppression [23]. Active piezoelectric dampers utilize piezoelectric materials to generate counteracting mechanical forces in response to structural strain [26]. The governing equations establish a relationship between mechanical deformation and the induced electrical actuation used for vibration suppression [27].

$$J\ddot{\theta}+\left(B+c_p\right)\dot{\theta}+\left(K+K_p\right)\theta=T_{gust} \tag{14}$$

The transfer function of the active piezoelectric damper is expressed as follows:

$$\frac{\theta(s)}{T_{gust}(s)}=\frac{1}{Js^2+\left(B+c_p\right)s+\left(K+K_p\right)} \tag{15}$$

2.3.6. Rotational Inertia Damper

The rotational inertia damper utilizes flywheel inertia to resist rapid changes in blade motion [28]. The rotational inertia damper employs a rotating flywheel to produce angular momentum that resists rapid changes in rotational motion. This inertial effect provides mechanical resistance that smooths blade motion and reduces vibration amplitudes [29].

$$\left(J_b + J_f\right)\ddot{\theta} + B\dot{\theta} + K\theta = T_{gust} \tag{16}$$

By implementing a rotational inertia damper in mechanical systems, engineers can achieve improved stability, safety, and longevity of the equipment, ultimately leading to better performance and reduced maintenance requirements [30].

The transfer function of the rotational inertia damper is represented by the following expression:

$$\frac{\theta(s)}{T_{gust}(s)} = \frac{1}{\left(J_b + J_f\right)s^2 + B_b \mathrm{s} + K_b} \tag{17}$$

2.3.7. Active Mass Driver Damper

The active mass driver damper employs motor-driven auxiliary mass motion to counteract vibration [29]. The active mass driver damper consists of a motor-driven auxiliary mass that moves in opposition to blade vibrations. Sensor feedback and control algorithms govern the mass motion, enabling real-time vibration mitigation [20].

$$J\ddot{\theta} + \left(B_b + c_{AMD}\right)\dot{\theta} + \left(K_b + K_{AMD}\right)\theta = T_{gust} \tag{18}$$

The transfer function of the active mass driver damper is expressed as follows:

$$\frac{\theta(s)}{T_{gust}(s)} = \frac{1}{Js^2 + \left(B_b + c_{AMD}\right)s + \left(K_b + K_{AMD}\right)} \tag{19}$$

2.3.8. Lorentz Torque Damper

The Lorentz torque damper generates contactless damping torque using electromagnetic induction [27]. The Lorentz torque damper generates a velocity-dependent resistive torque through electromagnetic induction without physical contact. This operating principle enables fast response, frictionless operation, and energy-efficient vibration suppression [4].

$$J\ddot{\theta} + B\dot{\theta} + K\theta + K_L\dot{\theta} = T_{gust} \tag{20}$$

The transfer function is:

$$\frac{\theta(s)}{T_{gust}(s)} = \frac{1}{Js^2 + \left(B + K_L\right)s + K} \tag{21}$$

The contactless operating principle eliminates frictional losses and mechanical wear.

2.3.9. Tuned Liquid Damper (TLD)

The tuned liquid damper dissipates vibration through controlled liquid sloshing motion [5]. The tuned liquid damper reduces structural vibrations through the controlled sloshing of liquid within a container [3]. The vibration control performance depends on the properties of the liquid and the geometric configuration of the tank [15].

$$J\ddot{\theta}+\left(B_b+c_L\right)\dot{\theta}+\left(K_b+K_L\right)\theta=T_{gust} \tag{22}$$

The transfer function of the tuned liquid damper can be expressed as follows:

$$\frac{\theta(s)}{T_{gust}(s)}=\frac{1}{J_b s^2+\left(B_b+c_L\right)s+\left(K_b+K_L\right)} \tag{23}$$

Symbol	Definition	Unit
(c_f)	Frictional clutch damping coefficient	N·m·s/rad
(c_{AH})	Active hydraulic damping coefficient	N·m·s/rad
(K_{AH})	Active hydraulic stiffness coefficient	N·m/rad
(c_{ED})	Electromagnetic damping coefficient	N·m·s/rad
(c_p)	Piezoelectric damping coefficient	N·m·s/rad
(K_p)	Piezoelectric stiffness coefficient	N·m/rad
(c_{AMD})	Active mass driver damping coefficient	N·m·s/rad
(K_{AMD})	Active mass driver stiffness coefficient	N·m/rad
(K_L)	Lorentz electromagnetic damping coefficient	N·m·s/rad
(c_L)	Tuned liquid damper damping coefficient	N·m·s/rad
(K_L)(TLD)	Liquid sloshing stiffness coefficient	N·m/rad

2.4. Added Mass and Inertia Modeling

The effective rotational inertia of the blade-damper coupled system is expressed as [24]:

$$W_d=m_d g \tag{24}$$

For the blade-damper coupled system, the effective rotational inertia becomes

$$J_{eq}=J_b+m_d r_d^2 \tag{25}$$

Symbol	Definition	Unit
m_d	Damper mass	kg
W_d	Damper weight	N
g	Gravitational acceleration (≈ 9.81)	m/s²
r_d	Radial distance of damper from blade root	m
J_{eff}	Effective rotational inertia of blade–damper system	kg·m²

Continued

J_b	Blade inertia	kg·m²
$m_d r_d^2$	Added inertia due to damper mass	kg·m²

Heavy dampers significantly increase effective rotational inertia and may alter the natural frequency of the blade system.

2.5. Energy Consumption Modeling

Energy consumption is modeled to quantify the power requirements of each damping technique during vibration suppression [23]. Conventional active and hydraulic dampers typically exhibit higher power demand, whereas the Lorentz torque damper operates primarily through electromagnetic induction and therefore requires minimal auxiliary energy [2].

$$E_d = \int_0^T P_d(t)\,\mathrm{d}t \tag{26}$$

For electrically actuated dampers (EMD, APD, AMD, AHD, and AFCD):

$$P_d(t) = V(t) I(t) \tag{27}$$

For hydraulic and mechanical active dampers, power is expressed as

$$P_d(t) = F_d(t)\dot{x}(t) \tag{28}$$

The Lorentz torque damper operates via electromagnetic induction using generator-coupled currents, requiring only minimal auxiliary power:

$$P_{lorentz} = K_e \omega^2 \tag{29}$$

This explains its consistently low energy consumption compared to fully active dampers.

Symbol	Definition	Unit
$P_d(t)$	Instantaneous damper power	W
$V(t)$	Applied voltage	V
$I(t)$	Actuator current	A
$F_d(t)$	Control force	N
$v(t)$	Blade linear velocity	m/s
ω	Blade angular velocity	rad/s
K_e	Electromagnetic coupling coefficient	N·m/A
T_L	Lorentz damping torque	N·m

The Lorentz torque damper requires minimal auxiliary energy because it operates primarily through induced electromagnetic interaction.

2.6. Overshoot and Rms Vibration Metrics

The percentage overshoot of a second-order system is expressed as [11]:

$$O_s\% = \frac{\theta_{max} - \theta_{ss}}{\theta_{ss}} \times 100\% \tag{30}$$

The *RMS* vibration amplitude is given by:

$$O_s\% = \mathrm{e}^{-\frac{\zeta\pi}{\sqrt{1-\zeta^2}} \times 100\%} \tag{31}$$

Together, these metrics help evaluate how well a damping system reduces both sudden and ongoing vibrations

$$\theta_{RMS} = \sqrt{\frac{1}{T}\int_0^T \theta^2(t)\,\mathrm{d}t} \tag{32}$$

The percentage *RMS* vibration reduction due to damping is defined as

$$RMS_{RED}\% = \frac{\theta_{RMS\ Undamped} - \theta_{RMS\ damped}}{\theta_{RMS\ Undamped}} \times 100\% \tag{33}$$

Active dampers reduce overshoot by increasing the effective damping ratio through control action.

Symbol	Definition	Unit
θ_{Max}	Maximum transient angular displacement	rad
θ_{ss}	Steady-state angular displacement	rad
ζ	Damping ratio	—
T	Observation time window	s
RMS	Root mean square vibration amplitude	rad
$\theta(t)$	Time-varying angular displacement	rad

2.7. Maintenance Demand Index

Maintenance demand is modeled as a function of mechanical complexity, actuator usage, and component failure rate [31]. This index provides a quantitative measure of the operational burden associated with each damping system over its service life [14].

$$MD = \alpha Nc + \beta E_a + \gamma\lambda f \tag{34}$$

Simplified comparative form used in this thesis:

$$MD_i = \frac{1}{T}\sum_{k=1}^{n} t_{ik} \tag{35}$$

where: t_{ik} is the maintenance time for damper *i*, T is the evaluation period

2.8. Cost Index Formulation

A cost index is formulated to integrate capital, operational, and maintenance costs into a single normalized economic metric [13]. This allows direct comparison of the economic feasibility of different damping strategies [25].

$$CI + C_{cap} + C_{op} + C_{maint} \tag{36}$$

For comparative evaluation across damping strategies, a normalized cost index is adopted:

Symbol	Definition	Unit
h_f	Failure rate	failures/year
C_i	Capital cost	USD
C_{op}	Operational cost	USD
C	Maintenance cost	USD
α, β, and γ	Weighting coefficients	—
M_i	Maintenance time for damper i	hours/year
T_e	Evaluation period	years

$$CI_{norm} = \frac{CI_i}{CI_{max}} \times 100\% \tag{37}$$

where CI_{norm} is the normalized cost index, CI_{max} is the maximum cost index, CI_i is the cost of each damper.

2.9. Frequency Response

The frequency response of the wind turbine blade under gust-induced excitation was analyzed using a second-order dynamic frequency response equation [26]. This equation describes how the blade system reacts to different excitation frequencies and helps evaluate resonance behavior, vibration attenuation capability, and overall dynamic stability of the damping systems.

$$\left|H(j\omega)\right| = \frac{1}{\sqrt{\left(1 - \frac{\omega}{\omega_n}\right)^2 + \left(2\zeta\omega_n\right)^2}} \tag{38}$$

where:

- ω represents the excitation frequency,
- ω_n is the natural frequency of the blade system,
- ζ is the damping ratio,
- $H(j\omega)$ represents the vibration response amplitude.

Dampers Type	Natural Frequency (ω_n)	Damping Ratio (\zeta)
Lorentz Damper	0.80	0.12
TMD Damper	0.70	0.08

Continued

Rotational Inertia Damper	0.70	0.07
Hydraulic Damper	0.70	0.065
Tuned Liquid Damper	0.68	0.06
Electromagnetic Damper	0.72	0.07
Piezoelectric Damper	0.70	0.075
Frictional Clutch Damper	0.65	0.05
Mass Driver Damper	0.70	0.07
Active Hydraulic Damper	0.68	0.075

3. Materials and Method

This study developed a unified MATLAB/Simulink framework to compare the proposed Lorentz Torque Damper with nine conventional wind turbine blade damping systems under identical operating conditions using both time-domain and frequency-domain excitations. The unified control structure, shown in Figure 1, provides a consistent and reliable platform for evaluating and comparing the dynamic performance of all damping systems based on key vibration control indices, including settling time, overshoot, vibration attenuation, and resonance suppression.

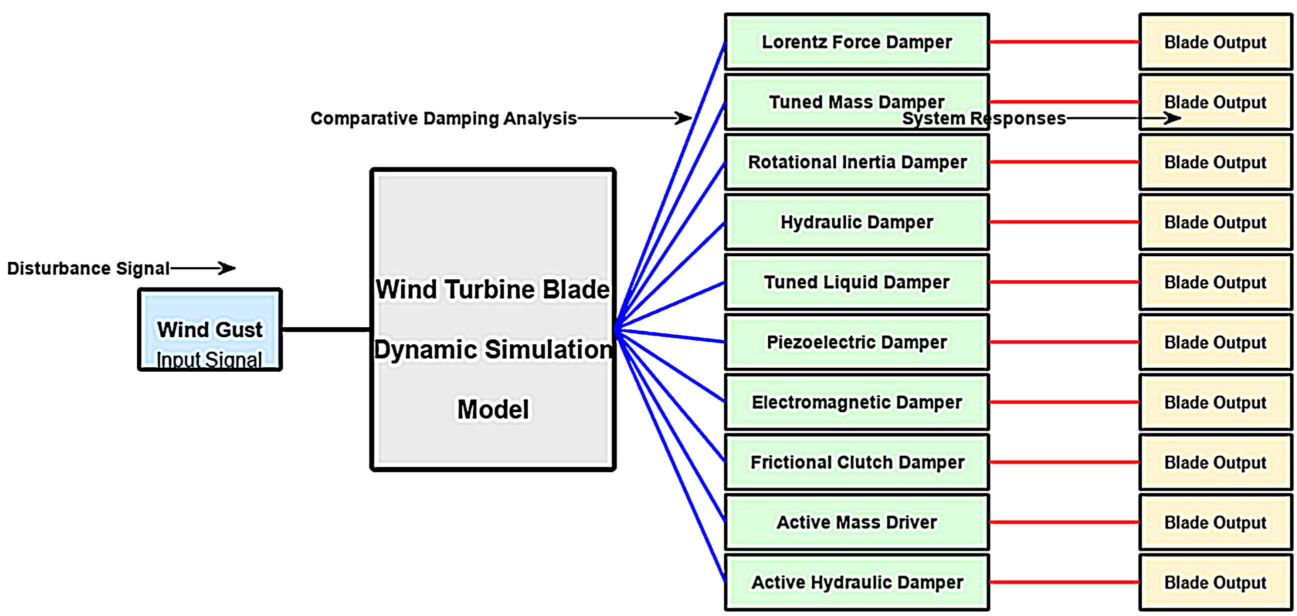

Figure 1. Simulink model architecture for comparative analysis Lorentz force based vibration control of wind turbine blade.

4. Results and Discussion

This section presents a detailed comparative evaluation of the Lorentz torque damper and the conventional damping systems under identical wind gust excitation conditions. The discussion focuses on the transient response characteristics, vibration suppression capability, energy efficiency, maintenance demand, and overall engineering suitability of the damping techniques for wind turbine blade applications.

4.1. Transient Response and Settling Time

Transient response analysis was performed to evaluate the capability of each damping system to suppress gust-induced oscillations and restore blade stability. The simulation results clearly show that the Lorentz torque damper consistently achieved faster settling time than all the conventional damping techniques considered in this study. The contactless electromagnetic operating principle eliminated mechanical lag, frictional delay, and hydraulic inertia effects that commonly limit the response speed of traditional damping systems.

4.1.1. Comparative Performance Analysis of the Lorentz Damper, Tuned Mass Damper, and Rotational Inertia Damper

This section compares the vibration suppression of the Lorentz, tuned mass, and rotational inertia dampers. The TMD uses an oscillating mass for slow disturbances, while the rotational inertia damper counters rapid motion with a spinning flywheel. Figure 2 and Figure 3 show their relative performance.

Figure 2 and Figure 3 compare the settling time of the proposed Lorentz torque damper with the Tuned Mass Damper and Rotational Inertia Damper. In both cases, the Lorentz damper achieved significantly faster stabilization, reducing settling time by 45.77% compared with the Tuned Mass Damper and by 44.52% compared with the Rotational Inertia Damper. These results highlight the superior transient response of the Lorentz torque damper, demonstrating its effectiveness in rapidly suppressing wind turbine blade vibrations under gust-induced loading.

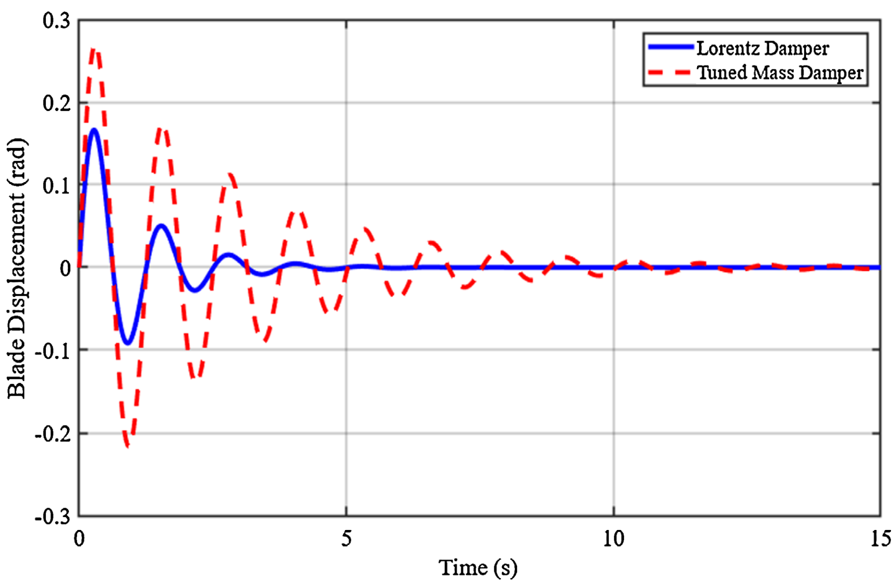

Figure 2. Lorentz and tuned mass damper.

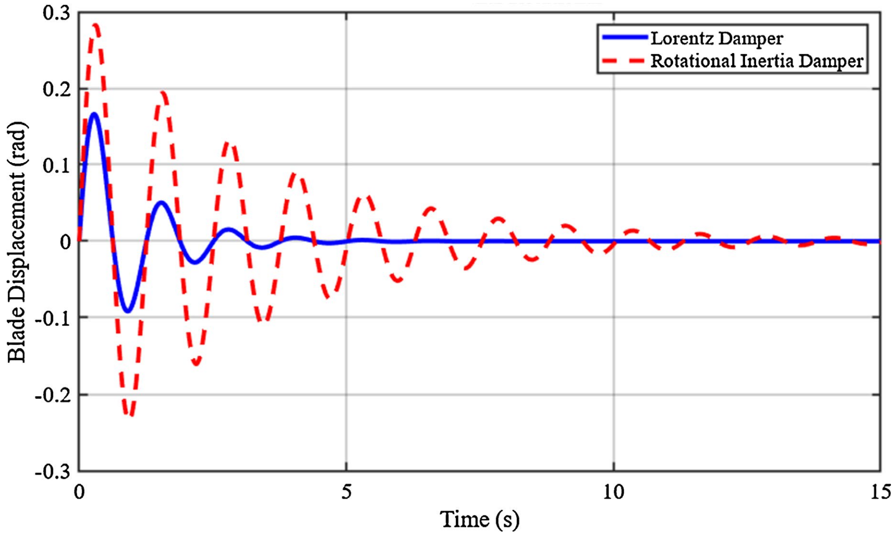

Figure 3. Lorentz and rotational damper.

4.1.2. Comparative Analysis of Lorentz, Hydraulic, and Tuned Liquid Dampers for Vibration Suppression

Hydraulic dampers dissipate energy through viscous fluid flow but may respond slowly to sudden loads. Figure 4 compares their performance with the Lorentz damper. Tuned liquid dampers reduce vibration via controlled liquid sloshing, as shown in Figure 5.

Figure 4 and Figure 5 compare the settling time of the proposed Lorentz torque damper with the Hydraulic Damper and Tuned Liquid Damper. In both comparisons, the Lorentz damper achieved faster stabilization, reducing settling time by 53.49% relative to the Hydraulic Damper and by 36.14% relative to the Tuned Liquid Damper. These findings further demonstrate the superior transient response of the Lorentz torque damper and its effectiveness in rapidly attenuating wind turbine blade vibrations.

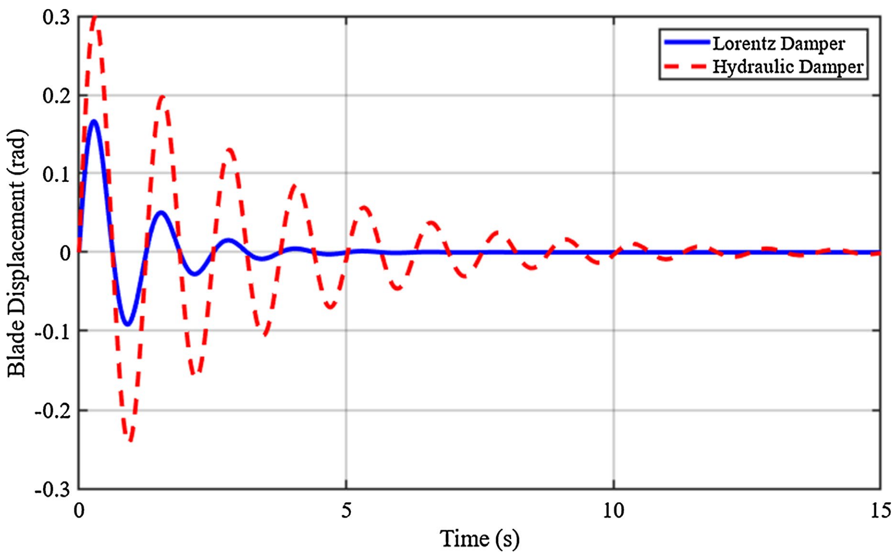

Figure 4. Lorentz and hydraulic damper.

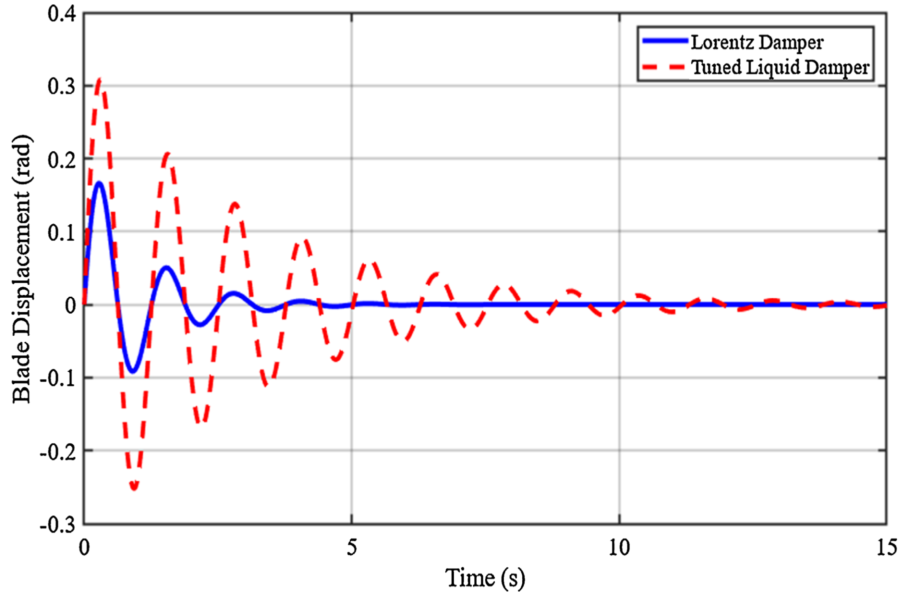

Figure 5. Tuned Liquid damper and Lorentz damper.

4.1.3. Comparative Performance Analysis: Lorentz Damper, Active Piezoelectric Damper, and Electromagnetic Damper

Electromagnetic dampers oppose motion using velocity-dependent eddy-current forces, compared with the Lorentz damper in Figure 6. Active piezoelectric dampers generate control forces via electrical-to-mechanical strain conversion. Figure 7 shows their dynamic response relative to the Lorentz damper.

Figure 6 and Figure 7 compare the settling time of the proposed Lorentz torque damper with the Active Piezoelectric Damper and Electromagnetic Damper. In both cases, the Lorentz damper achieved faster stabilization, reducing settling time by 45.91% relative to the Active Piezoelectric Damper and by 27.83% relative to the Electromagnetic Damper. These results further confirm the superior

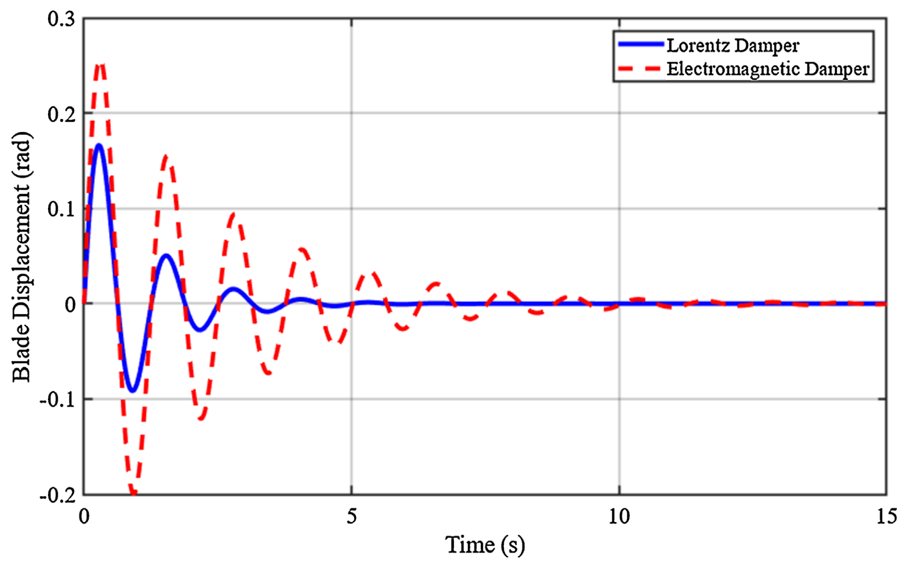

Figure 6. Lorentz and active electromagnetic damper.

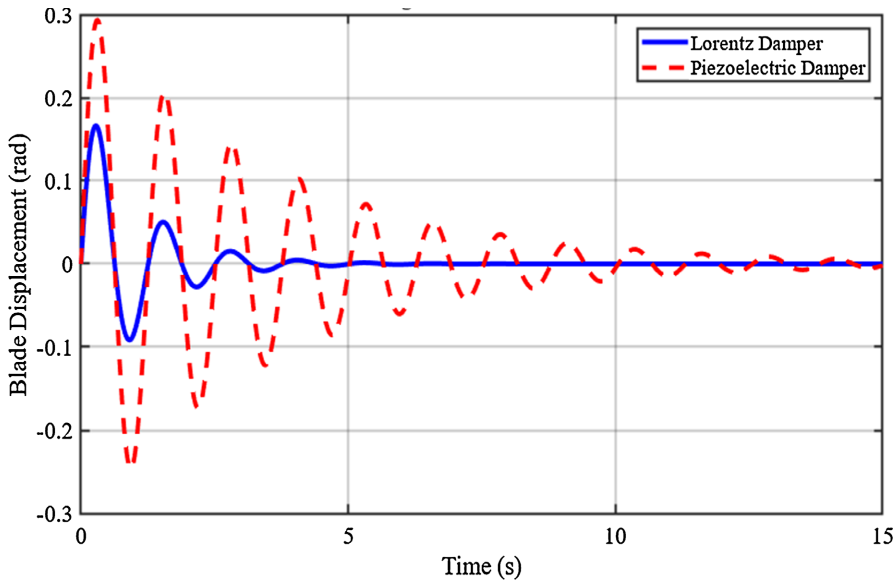

Figure 7. Lorentz and piezoelectric damper.

transient response of the Lorentz torque damper and its effectiveness in rapidly suppressing wind turbine blade vibrations.

4.1.4. Comparative Performance Analysis of the Lorentz Damper, Active Mass Driver Damper, and Active Hydraulic Damper

Figure 8 and Figure 9 present the comparative performance analysis of the Lorentz damper, Active Mass Driver (AMD) damper, and Active Hydraulic Damper (AHD). The Active Mass Driver damper suppresses vibrations using a motor-driven auxiliary mass, while the Active Hydraulic Damper utilizes hydraulic actuation to counter oscillatory motion. Compared with both conventional damping systems, the Lorentz damper demonstrates superior vibration suppression

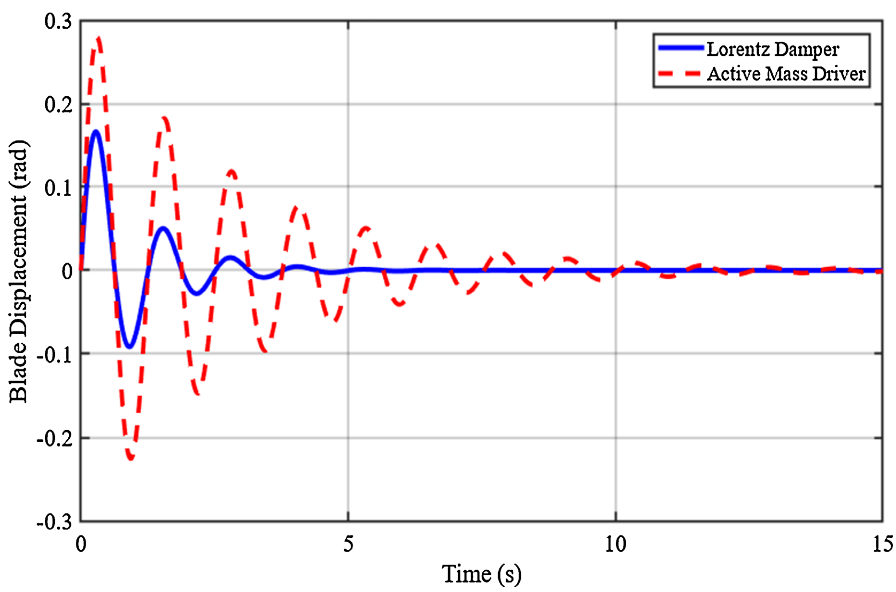

Figure 8. Active mass driver damper and Lorentz damper.

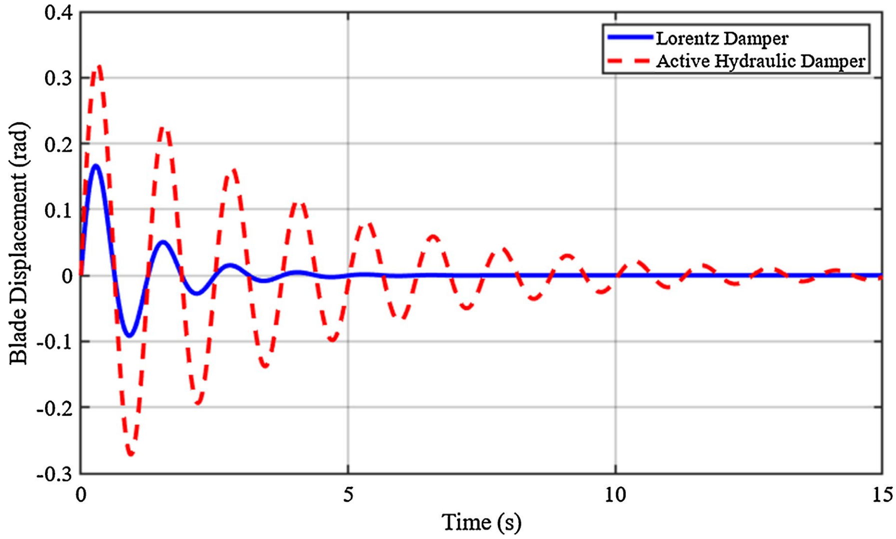

Figure 9. Active Hydraulic damper and Lorentz damper.

performance, achieving faster response and improved damping efficiency with lower operational demands.

Figure 8 and Figure 9 compare the settling time performance of the proposed Lorentz torque damper with the Active Frictional Clutch Damper and Active Mass Driver Damper. The Lorentz damper consistently achieves faster stabilization, reducing settling time by 48.43% compared with the Active Frictional Clutch Damper and by 42.94% compared with the Active Mass Driver Damper. These results confirm the superior transient response of the Lorentz torque damper in rapidly attenuating wind turbine blade vibrations.

4.1.5. Comparative Analysis of Active Frictional Clutch Damper and Lorentz Damper

Figure 10 presents a comparative analysis between the Active Frictional Clutch

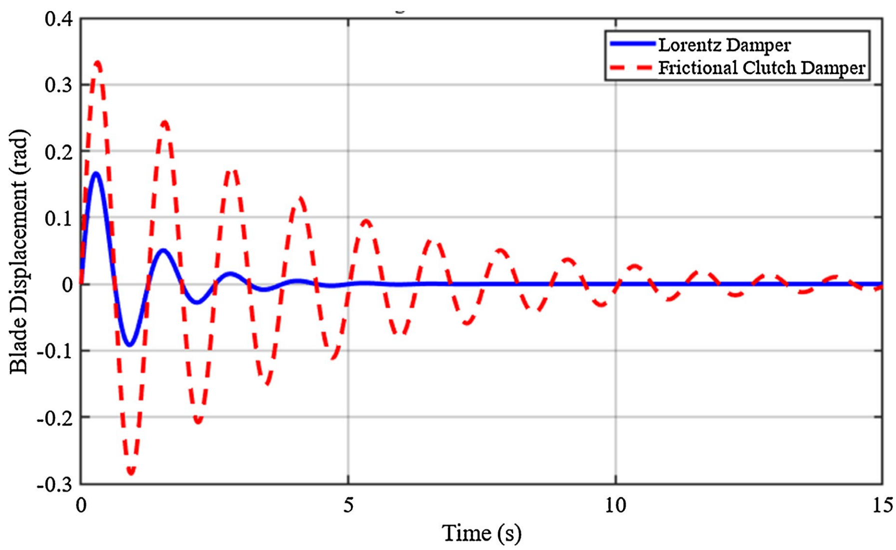

Figure 10. Active frictional damper and Lorentz damper.

Damper (AFCD) and the Lorentz damper under transient excitation. The AFCD reduces vibration through frictional energy dissipation but is affected by wear, engagement delay, and higher energy losses, leading to reduced damping efficiency. In contrast, the Lorentz damper provides faster and more precise vibration suppression, demonstrating superior transient response and overall damping performance under gust-induced loading conditions.

The Lorentz torque damper achieves about 60.02% faster settling time than the Active Frictional Clutch Damper due to its contactless electromagnetic design, which removes frictional delays and energy losses. In contrast, the AFCD suffers from response lag caused by frictional engagement, reducing its damping efficiency under variable excitation. Overall, the Lorentz damper demonstrates superior transient performance and more effective vibration suppression for wind turbine applications.

4.2. Frequency Response Analysis

Frequency response analysis was conducted to evaluate the effectiveness of each damping system under fluctuating wind gust excitation. The Lorentz torque damper consistently demonstrated lower resonance amplitude, improved oscillation suppression, and faster decay characteristics compared with the conventional damping techniques. The electromagnetic operating principle of the Lorentz damper enabled adaptive response over a wider frequency range, thereby improving structural stability during turbulent wind conditions.

4.2.1. Frequency Response Comparison of Tuned Mass and Rotational Inertia Dampers

Figure 11 and Figure 12 illustrate the frequency response characteristics of the tuned mass damper, rotational inertia damper, and Lorentz force damper under fluctuating wind gust loading. Figure 11 shows the comparison between the tuned mass damper and the Lorentz damper, while Figure 12 presents the comparison between the rotational inertia damper and the Lorentz damper.

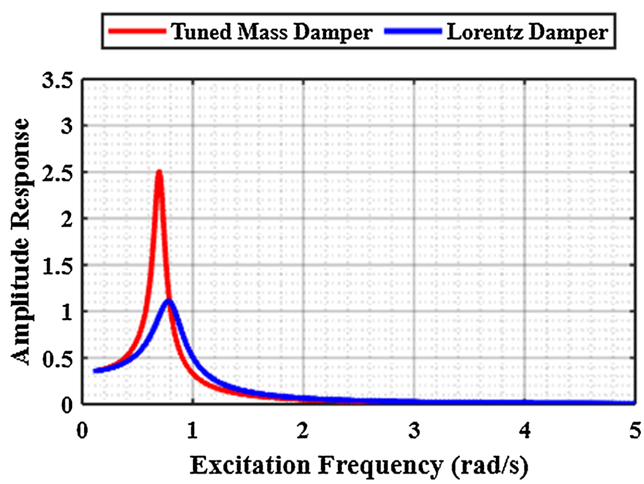

Figure 11. Frequency response of the tuned mass damper and the Lorentz damper.

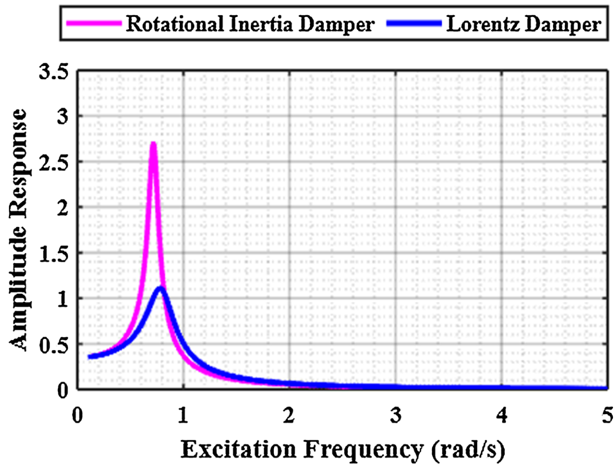

Figure 12. Frequency response of the rotational inertia damper and the Lorentz damper.

The tuned mass damper effectively reduces vibrations near its tuned resonance frequency but loses effectiveness with varying wind gusts, whereas the Lorentz force damper provides dynamic electromagnetic counterforces for improved stabilization and faster response under turbulent conditions.

4.2.2. Frequency Response Comparison of Hydraulic and Tuned Liquid Dampers

Figure 13 and Figure 14 provide comparative analyses of the vibration suppression capabilities of the hydraulic and tuned liquid dampers relative to the Lorentz damper. Figure 13 evaluates the hydraulic damper and Lorentz damper under wind gust disturbances, while Figure 14 compares the tuned liquid damper with the Lorentz damper.

The study highlights that while the hydraulic damper's energy dissipation is hindered by fluid inertia during rapid fluctuations, the Lorentz force damper provides lower resonance amplitude, quicker stabilization, and enhanced vibration suppression performance.

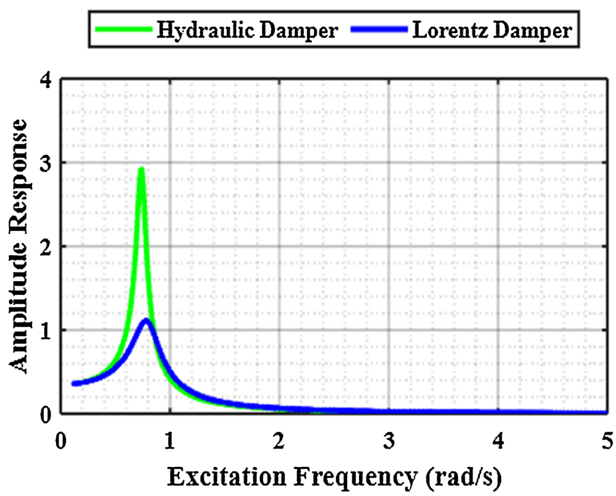

Figure 13. Frequency response of the hydraulic damper and the Lorentz damper.

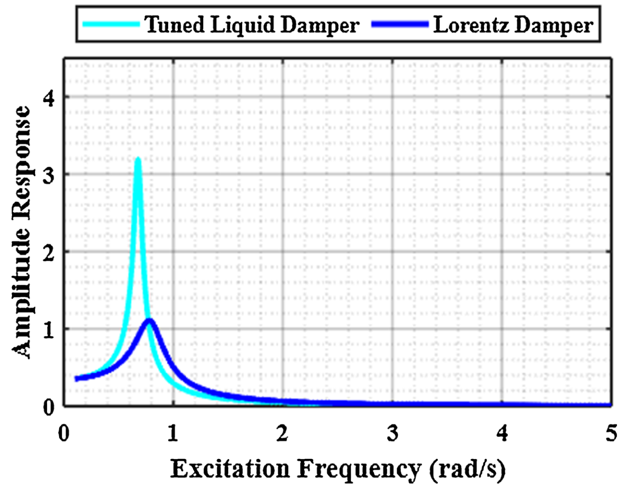

Figure 14. Frequency response of the tuned liquid damper and the Lorentz damper.

4.2.3. Frequency Response Comparison of Electromagnetic and Piezoelectric Dampers

Figure 15 and **Figure 16** illustrate the frequency response comparisons involving

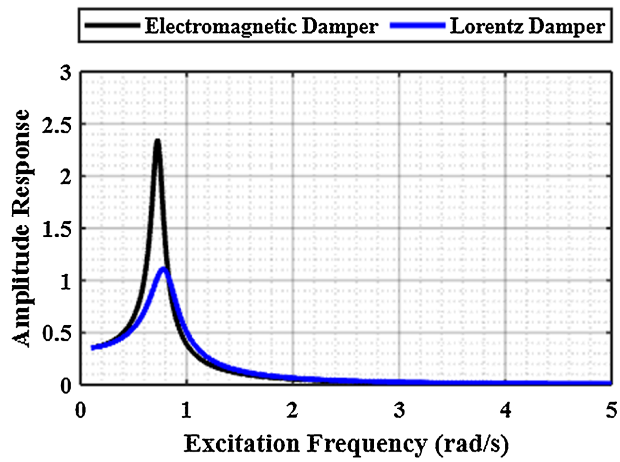

Figure 15. Frequency response of the electromagnetic damper and the Lorentz damper.

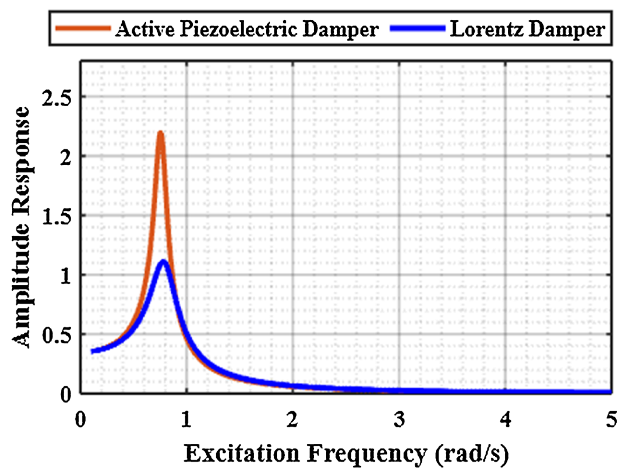

Figure 16. Frequency response of the active piezoelectric damper and the Lorentz damper.

electromagnetic and active piezoelectric dampers with the Lorentz damper. Figure 15 compares the conventional electromagnetic damper with the Lorentz damper, whereas Figure 16 presents the comparison between the active piezoelectric damper and the Lorentz damper.

The lorentz force damper outperforms the conventional electromagnetic damper by providing lower resonance amplitude, quicker stabilization, and improved vibration control across a wider frequency range.

4.2.4. Frequency Response Comparison of Active Mass Driver and Active Hydraulic Dampers

Figure 17 and Figure 18 illustrate the vibration attenuation performance of the active mass driver damper and active hydraulic damper compared with the Lorentz damper. Figure 17 presents the active mass driver damper comparison, while Figure 18 shows the active hydraulic damper comparison under turbulent wind excitation.

The Lorentz force damper demonstrates quicker response and improved resonance suppression compared with both active damping systems.

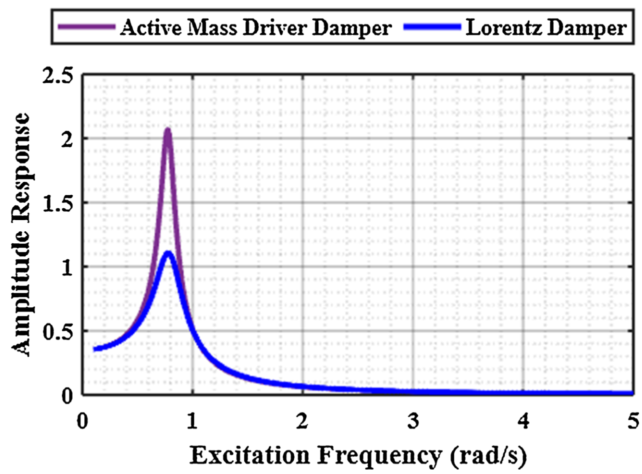

Figure 17. Frequency response of active mass driver damper and Lorentz damper.

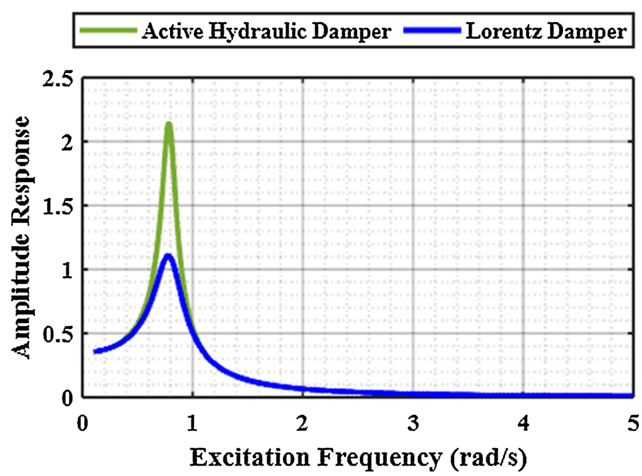

Figure 18. Frequency response of the active mass driver damper and the Lorentz damper.

4.2.5. Frequency Response Comparison of Active Frictional Clutch Damper

Figure 19 evaluates the effectiveness of the active frictional clutch damper compared with the Lorentz force damper in reducing resonance amplitude and improving blade stability under varying wind gust excitation.

The comparison presented in Figure 19 reveals that the Lorentz force damper provides superior vibration suppression, faster stabilization, and enhanced operational stability across all excitation frequencies.

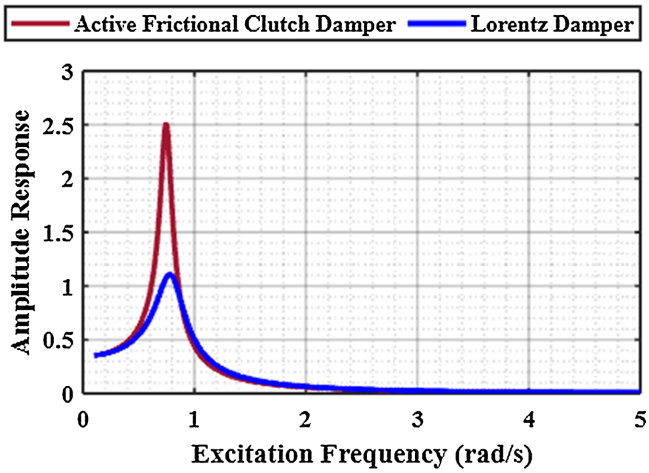

Figure 19. Frequency response of the active frictional clutch damper and the Lorentz damper.

4.3. RMS Vibration Comparison

The RMS vibration analysis further confirms the superior damping capability of the Lorentz torque damper, which achieved the greatest reduction in sustained vibration amplitude among all evaluated damping systems. Figure 20 shows the RMS vibration reduction comparison for all damping techniques considered in this study.

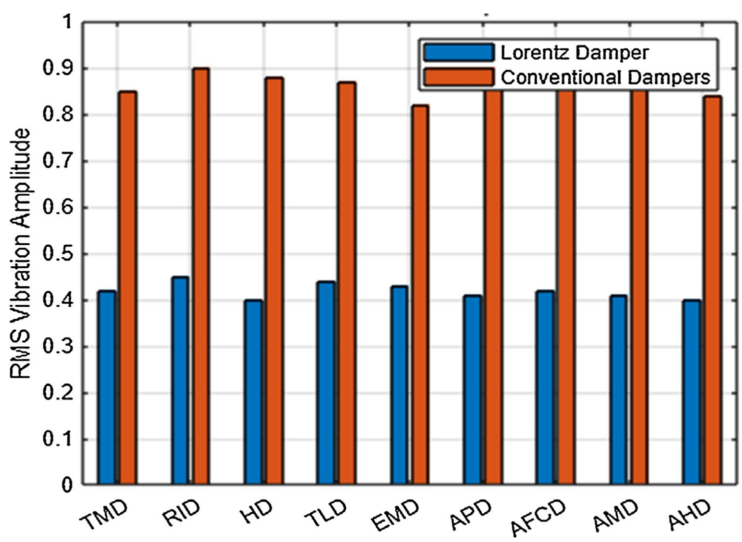

Figure 20. RMS vibration reduction comparison.

Figure 20 demonstrates that the Lorentz torque damper minimizes RMS vibration, thereby improving structural reliability and reducing fatigue loading.

4.4. Settling Time Comparison

Settling time analysis demonstrated that the Lorentz torque damper restored blade stability significantly faster than conventional damping techniques. Figure 21 presents the settling time comparison for all damping systems investigated.

Figure 21 illustrates that the Lorentz torque damper provides the fastest stabilization response following gust-induced disturbances.

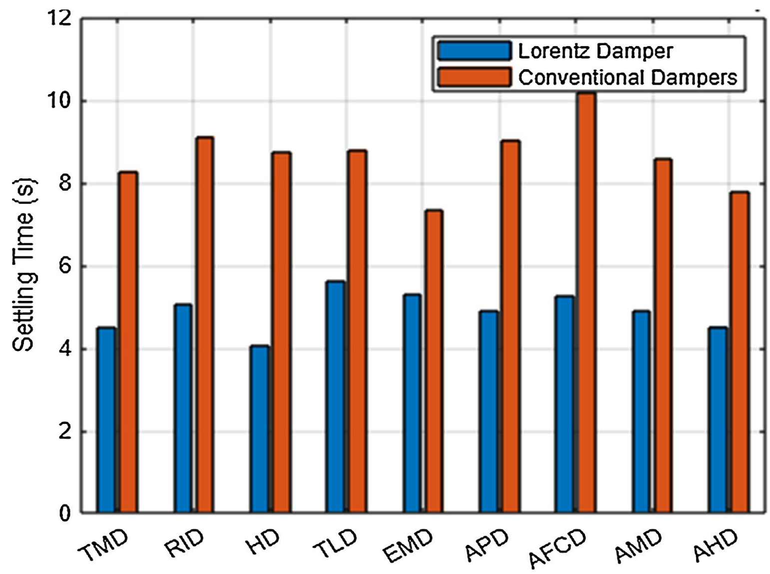

Figure 21. Settling time comparison.

4.5. Overshoot Comparison

The Lorentz torque damper produced the lowest transient overshoot among all damping systems evaluated. Figure 22 presents the overshoot comparison for the investigated damping techniques.

Figure 22 shows that the Lorentz torque damper minimizes transient stress concentration by maintaining the lowest overshoot response.

4.6. Added Weight Comparison

The Lorentz torque damper introduced minimal additional structural mass compared with conventional passive damping systems. Figure 23 presents the added weight comparison for all damping systems.

Figure 23 shows that the Lorentz torque damper preserves blade dynamic properties because of its lightweight design.

4.7. Energy Consumption Comparison

The energy consumption analysis indicates that the Lorentz torque damper requires significantly lower operational energy than active hydraulic, active mass

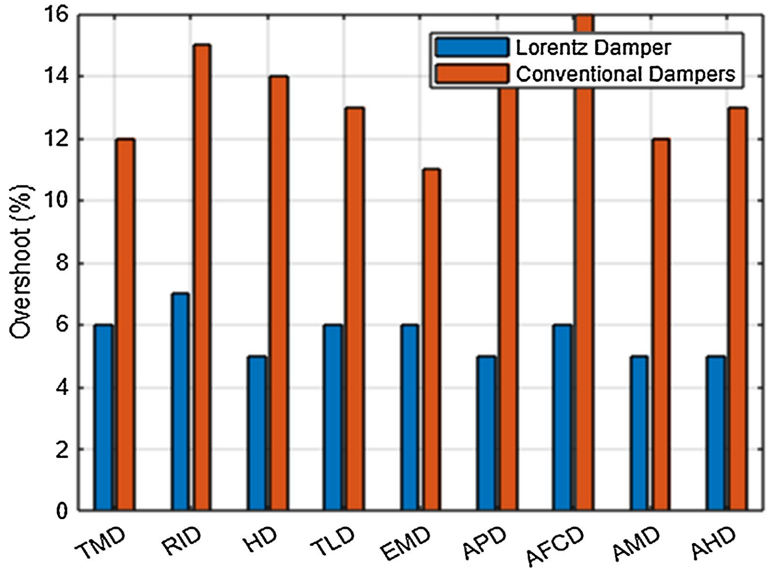

Figure 22. Overshoot comparison.

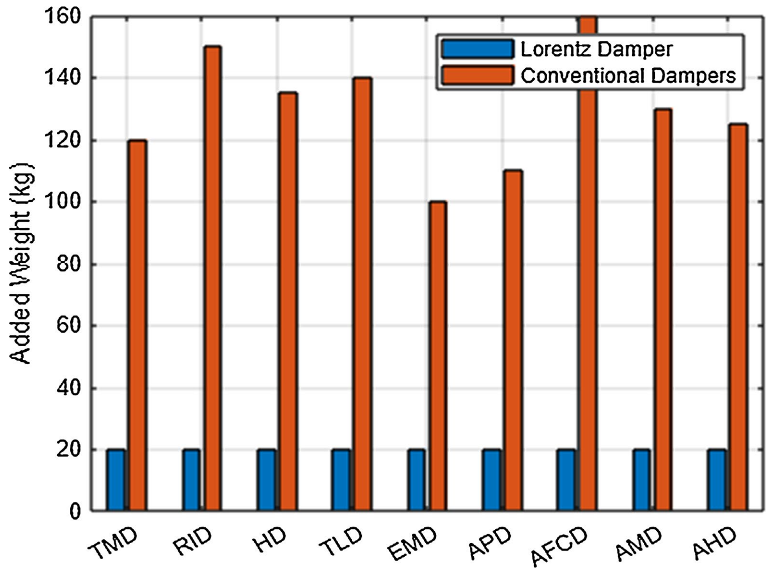

Figure 23. Added weight comparison.

driver, and piezoelectric damping systems. Figure 24 presents the energy consumption comparison among the damping techniques.

Figure 24 shows that the Lorentz torque damper consumes the least operational energy, supporting sustainable and cost-effective turbine operation.

4.8. Maintenance Demand Comparison

The Lorentz torque damper exhibited the lowest maintenance demand among all evaluated damping systems. Figure 25 presents the maintenance demand comparison for the investigated dampers.

Figure 25 illustrates that the Lorentz torque damper requires minimal maintenance because of its contactless electromagnetic operating principle.

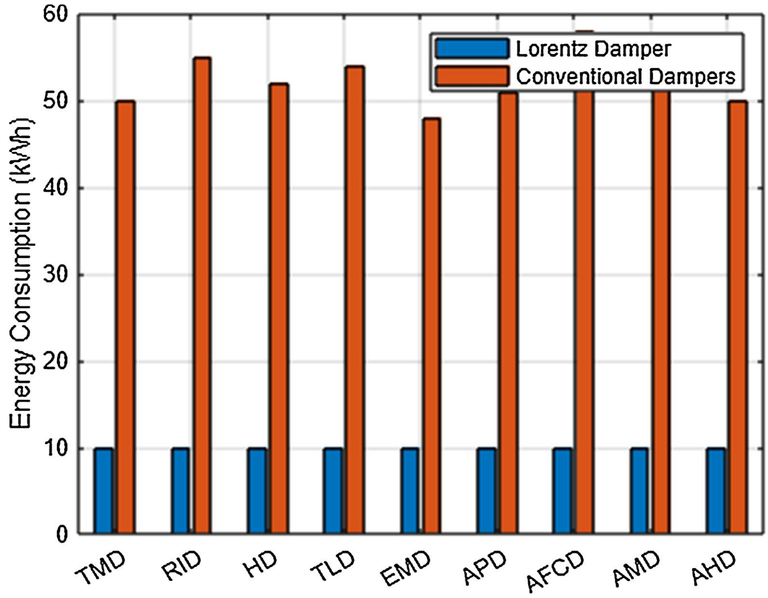

Figure 24. Energy consumption comparison.

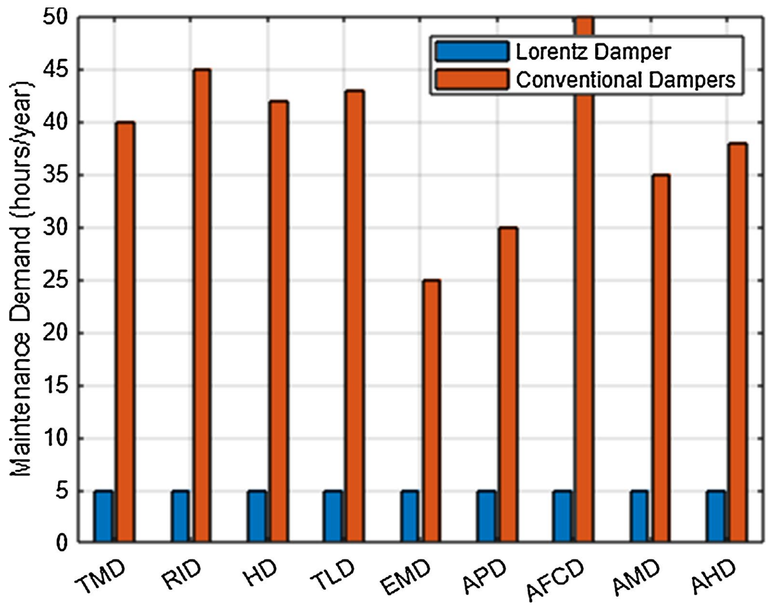

Figure 25. Maintenance demand comparison.

4.9. Vibration Suppression Efficiency

The vibration suppression efficiency comparison demonstrated that the Lorentz torque damper achieved the highest vibration attenuation performance. Figure 26 presents the vibration suppression efficiency comparison for all damping systems.

Figure 26 shows that the Lorentz torque damper provides the highest overall vibration suppression efficiency.

4.10. Cost Index Comparison

The normalized cost index analysis demonstrated that the Lorentz torque damper offers improved economic feasibility compared with conventional active damping systems. Figure 27 presents the cost index comparison of the investigated damping techniques.

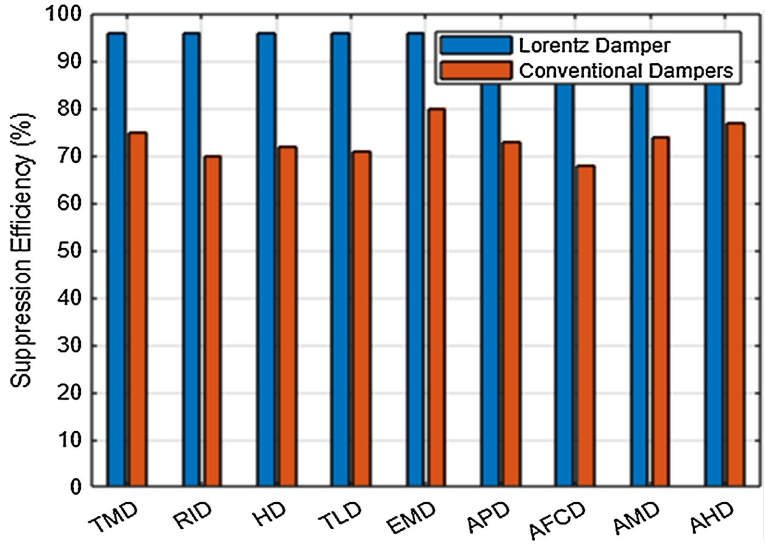

Figure 26. Vibration suppression efficiency comparison.

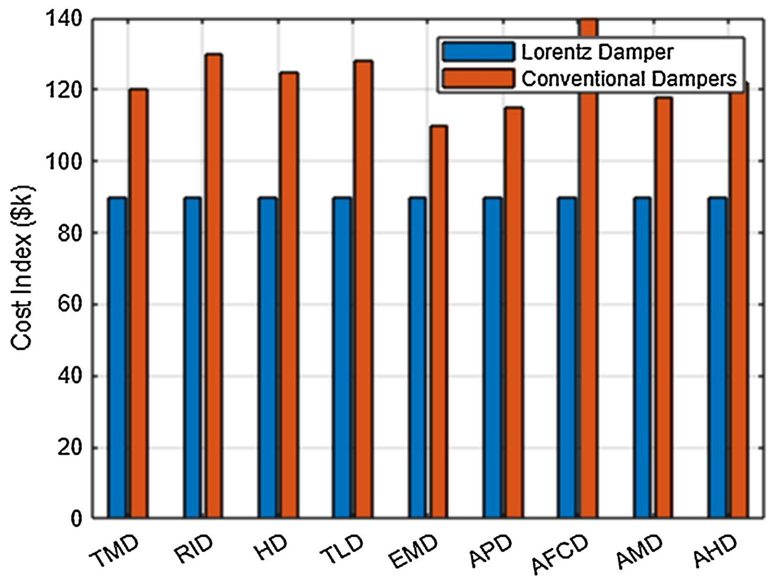

Figure 27. Cost index comparison.

Figure 27 shows that although electromagnetic systems may have relatively higher initial installation cost, the Lorentz torque damper achieves lower long-term operational cost because of reduced maintenance and energy consumption.

4.11. Model Validation

The developed MATLAB/Simulink model was validated by comparing the predicted natural frequency with benchmark data reported in previous studies. The simulated natural frequency of 2.212 Hz closely matched the benchmark frequency of 2.100 Hz, resulting in a validation error of approximately 5.32%. This confirms the accuracy and reliability of the developed blade vibration model.

4.12. Engineering Implications

The results demonstrate that the Lorentz torque damper offers superior performance for modern wind turbine vibration suppression by providing rapid transient response, improved vibration attenuation, and enhanced operational stability. The system also achieves lower energy consumption, reduced maintenance demand, and minimal additional structural mass compared with conventional damping techniques. These advantages make the Lorentz torque damper highly suitable for large-scale offshore wind turbine applications where reliability, efficiency, and ease of maintenance are essential.

5. Conclusion

The study successfully demonstrated the effectiveness of the Lorentz torque damper for vibration suppression in wind turbine blade systems through a comprehensive comparative analysis with nine conventional damping techniques. This study presented a comparative evaluation of a Lorentz torque damper against nine conventional damping techniques for vibration suppression in wind turbine blade systems using a unified MATLAB/Simulink framework. The results demonstrated that the Lorentz torque damper achieved superior transient response, reduced RMS vibration amplitude, lower overshoot, reduced maintenance demand, minimal added mass, and lower operational energy consumption compared with the conventional damping systems. The developed model further demonstrated strong agreement with benchmark frequency data, thereby validating the accuracy of the proposed dynamic framework. The contactless electromagnetic operating principle of the Lorentz torque damper eliminates frictional wear and enables rapid adaptive vibration suppression under turbulent wind conditions. The overall findings indicate that the Lorentz torque damper represents an efficient, reliable, and economically attractive solution for advanced vibration control in modern wind turbine blade systems. Future work should focus on experimental validation, real-time controller implementation, and large-scale deployment analysis for offshore wind energy applications.

Conflicts of Interest

The authors declare no conflicts of interest regarding the publication of this paper.

References

[1] Qansh, H. (2022) Aerodynamic Analysis on Modified Horizontal-Axis-Wind-Turbine. Ph.D. Thesis, University of Sheffield. https://etheses.whiterose.ac.uk/30630/

[2] Martynowicz, P. (2022) Experimental Study on the Optimal-Based Vibration Control of a Wind Turbine Tower Using a Small-Scale Electric Drive with MR Damper Support. *Energies*, **15**, Article 9530. https://doi.org/10.3390/en15249530

[3] Li, J., Zhu, S., Zhang, J., Ma, R. and Zuo, H. (2024) Vibration Control of Offshore Wind Turbines with a Novel Energy-Adaptive Self-Powered Active Mass Damper. *Engineering Structures*, **302**, Article 117450. https://doi.org/10.1016/j.engstruct.2024.117450

[4] Hashemi, A., Jang, J. and Hosseini-Hashemi, S. (2022) Smart Active Vibration Control System of a Rotary Structure Using Piezoelectric Materials. *Sensors*, **22**, Article 5691. https://doi.org/10.3390/s22155691

[5] Liu, Z., Wang, C. and Zhang, D. (2025) Study on Vibration Control of Wind Turbine with an Optimised Eddy Current Tuned Rolling Cylinder Damper. *Structural Control and Health Monitoring*, **2025**, Article ID: 6726023. https://doi.org/10.1155/stc/6726023

[6] Wang, C. and Chiang, M. (2016) A Novel Pitch Control System of a Large Wind Turbine Using Two-Degree-of-Freedom Motion Control with Feedback Linearization Control. *Energies*, **9**, Article 791. https://doi.org/10.3390/en9100791

[7] Liang, D., Song, C., Liang, S., Wang, S., Li, Y. and Zhou, Z. (2021) Design and Performance Analysis of Blades Based on the Equal-Variable Circulation Method. *Frontiers in Energy Research*, **9**, Article ID: 790622. https://doi.org/10.3389/fenrg.2021.790622

[8] Lopez-Lopez, A., Robles-Ocampo, J.B., Sevilla-Camacho, P.Y., Lastres-Danguillecourt, O., Muniz, J., Perez-Sariñana, B.Y., *et al.* (2020) Dynamic Instability of a Wind Turbine Blade Due to Large Deflections: An Experimental Validation. *Strojniški Vestnik—Journal of Mechanical Engineering*, **66**, 523-533. https://doi.org/10.5545/sv-jme.2020.6678

[9] Zhang, J., Gong, Z., Zhang, X., Guo, L. and Hu, D. (2018) Dynamic Analysis of Offshore Wind Turbine Blades under the Action of Wind Shear and Fluctuating Wind. *Journal of Vibroengineering*, **20**, 1511-1521. https://doi.org/10.21595/jve.2017.19069

[10] Kocabiyikoğlu, Z.U. (2020) Principles of Electromechanical Energy Conversion. In: Kocabiyikoğlu, Z.U., Ed., *Electromechanical Energy Conversion*, CRC Press, 103-136. https://doi.org/10.1201/9780429317637-3

[11] Liu, Y., Wang, X. and Li, Y. (2020) Distributed Piezoelectric Actuator Layout-Design for Active Vibration Control of Thin-Walled Smart Structures. *Thin-Walled Structures*, **147**, Article 106530. https://doi.org/10.1016/j.tws.2019.106530

[12] Di Paolo, M., Nuzzo, I., Caterino, N. and Georgakis, C.T. (2021) A Friction-Based Passive Control Technique to Mitigate Wind Induced Structural Demand to Wind Turbines. *Engineering Structures*, **232**, Article 111744. https://doi.org/10.1016/j.engstruct.2020.111744

[13] Thiele, F., Wisbacher, S., Diaconescu, S., Ossmann, D. and Pfifer, H. (2023) Periodic LQG Wind Turbine Control with Adaptive Load Reduction. *IFAC-PapersOnLine*, **56**, 7674-7679. https://doi.org/10.1016/j.ifacol.2023.10.1168

[14] Rosół, M. and Martynowicz, P. (2016) Implementation of the LQG Controller for a Wind Turbine Tower-Nacelle Model with an Mr Tuned Vibration Absorber. *Journal of Theoretical and Applied Mechanics*, **54**, 1109-1123. https://doi.org/10.15632/jtam-pl.54.4.1109

[15] Amer, Y.A., EL-Sayed, A.T. and Agwa, M.M. (2024) Controlling Wind Turbine Tower Vibration under External Force by Applying Control Systems Combination. *Scientific Reports*, **14**, Article No. 18597. https://doi.org/10.1038/s41598-024-68237-6

[16] Mendecka, B. and Lombardi, L. (2019) Life Cycle Environmental Impacts of Wind

Energy Technologies: A Review of Simplified Models and Harmonization of the Results. *Renewable and Sustainable Energy Reviews*, **111**, 462-480. https://doi.org/10.1016/j.rser.2019.05.019

[17] Hussain, T., Min Ullah, F.U., Muhammad, K., Rho, S., Ullah, A., Hwang, E., *et al.* (2021) Smart and Intelligent Energy Monitoring Systems: A Comprehensive Literature Survey and Future Research Guidelines. *International Journal of Energy Research*, **45**, 3590-3614. https://doi.org/10.1002/er.6093

[18] Li, Y., Huang, X., Tee, K.F., Li, Q. and Wu, X. (2020) Comparative Study of Onshore and Offshore Wind Characteristics and Wind Energy Potentials: A Case Study for Southeast Coastal Region of China. *Sustainable Energy Technologies and Assessments*, **39**, Article 100711. https://doi.org/10.1016/j.seta.2020.100711

[19] Gönül, Ö., Duman, A.C., Deveci, K. and Güler, Ö. (2021) An Assessment of Wind Energy Status, Incentive Mechanisms and Market in Türkiye. *Engineering Science and Technology, an International Journal*, **24**, 1383-1395. https://doi.org/10.1016/j.jestch.2021.03.016

[20] Elhaji, E.M. (2018) Modeling and Control of Wind Turbine to Damp the Power Oscillation. In: Okedu, K.E., Ed., *Stability Control and Reliable Performance of Wind Turbines*, InTech, 1-10. https://doi.org/10.5772/intechopen.74835

[21] Kavade, R.K., Sonekar, M.M., Choudhari, D.S., Malwe, P.D., Sherje, N.P., Ansari, M.A., *et al.* (2024) Investigation on Fixed Pitch Darrieus Vertical Axis Wind Turbine. *AIP Advances*, **14**, Article 075025. https://doi.org/10.1063/5.0203609

[22] Sumair, M., Aized, T., Gardezi, S.A.R., Rehman, S.M.S. and ur Rehman, S.U. (2021) Investigation of Wind Shear Coefficients and Their Effect on Annual Energy Yields along the Coastal Sites of Pakistan. *Energy Exploration & Exploitation*, **39**, 2169-2190. https://doi.org/10.1177/0144598720930422

[23] Machado, M.R. and Dutkiewicz, M. (2024) Wind Turbine Vibration Management: An Integrated Analysis of Existing Solutions, Products, and Open-Source Developments. *Energy Reports*, **11**, 3756-3791. https://doi.org/10.1016/j.egyr.2024.03.014

[24] Zhang, Z., Li, X., Larsen, T.G., Sun, T. and Yang, Q. (2024) Pole-Placement-Based Calibration of an Electromagnetically Realizable Inerter-Based Vibration Absorber (IDVA) for Rotating Wind Turbine Blades. *Structural Control and Health Monitoring*, **2024**, Article ID: 7255774. https://doi.org/10.1155/2024/7255774

[25] Zhu, C. and Li, Y. (2018) Reliability Analysis of Wind Turbines. In: Okedu, K.E., Ed., *Stability Control and Reliable Performance of Wind Turbines*, InTech, 376-389. https://doi.org/10.5772/intechopen.74859

[26] Okokpujie, I.P., Akinlabi, E.T., Udoye, N.E. and Okokpujie, K. (2021) Comprehensive Review of the Effects of Vibrations on Wind Turbine during Energy Generation Operation, Its Structural Challenges and Way Forward. In: Akinlabi, E., Ramkumar, P. and Selvaraj, M., Eds., *Lecture Notes in Mechanical Engineering*, Springer, 935-948. https://doi.org/10.1007/978-981-15-4488-0_79

[27] Bin, G., Li, X., Shen, Y. and Wang, W. (2018) Development of Whole-Machine High Speed Balance Approach for Turbomachinery Shaft System with N + 1 Supports. *Measurement*, **122**, 368-379. https://doi.org/10.1016/j.measurement.2018.02.035

[28] Chong, C.H., Rigit, A.R.H. and Ali, I. (2021) Wind Turbine Modelling and Simulation Using Matlab/Simulink. *IOP Conference Series: Materials Science and Engineering*, **1101**, Article 012034. https://doi.org/10.1088/1757-899x/1101/1/012034

[29] Ma, H., Zhao, Q., Zhao, X., Han, Q. and Wen, B. (2015) Dynamic Characteristics Analysis of a Rotor-Stator System under Different Rubbing Forms. *Applied Mathe-*

matical Modelling, **39**, 2392-2408. https://doi.org/10.1016/j.apm.2014.11.009

[30] Panagiotis, C.J. (2024) Vibrations and Damping Mechanisms in Wind Turbines: Challenges and Advances in Material Design and Control Systems. *International Advanced Research Journal in Science*, *Engineering and Technology*, **11**, 1-19.

[31] Fitzgerald, B., Basu, B. and Nielsen, S.R.K. (2013) Active Tuned Mass Dampers for Control of In-Plane Vibrations of Wind Turbine Blades. *Structural Control and Health Monitoring*, **20**, 1377-1396. https://doi.org/10.1002/stc.1524